Biosensors and Bioelectronics 168 (2020) 112516

Contents lists available at ScienceDirect

Biosensors and Bioelectronics

journal homepage: http://www.elsevier.com/locate/bios

Ultrasensitive aptasensor for isolation and detection of circulating tumor cells based on CeO_2@Ir nanorods and DNA walker

Huawei Shen [a,b,1], Wuquan Deng [c,1], Yirui He [d], Xinrun Li [d], Jinlin Song [e], Rui Liu [d], Hua liu [f], Gangyi Yang [d], Ling Li [a,*]

[a] Key Laboratory of Medical Diagnostics of Ministry of Education, Department of Laboratory Medicine, Chongqing Medical University, Chongqing, 400016, China
[b] Clinical Laboratory Medicine Center, Chongqing Hospital of Traditional Chinese Medicine, Chongqing, 400021, China
[c] Chongqing Emergency Medical Center, Chongqing, 400014, China
[d] Department of Endocrinology, The Second Affiliated Hospital, Chongqing Medical University and Chongqing Clinical Research Center for Geriatrics, Chongqing, 400010, China
[e] College of Stomatology, Chongqing Key Laboratory for Oral Diseases and Biomedical Science, Chongqing Medical University, Chongqing, 401147, China
[f] Department of Pediatrics, University of Mississippi Medical Center, 2500 North State Street, Jackson, MS, MS 39216-4505, USA

ARTICLE INFO

Keywords:
Electrochemical biosensor
Aptamer
Nanorods
Enzyme-free DNA walker
Circulating tumor cells

ABSTRACT

Herein, based on dual signal amplification by CeO_2@Ir nanorods (Ce@IrNRs) and enzyme-free DNA walker, a novel electrochemical aptasensor was developed for simultaneous isolation and detection of circulating tumor cells (CTCs). A membrane protein MUC1-targeting aptamer was used to specifically recognize and capture MCF-7 cells. Uracil DNA glycosylase could hydrolyze deoxyuracils of the aptamer to isolate the captured cells. Novel Ce@IrNRs with large surface area and high peroxidase activity were synthesized to amplify the signal, and the enzyme-free DNA walker was applied to release more signal probes combined with Ce@IrNRs. Furthermore, to reduce steric hindrance by cells, the signal probes rather than the target cells, were directly combined with the electrode. The aptasensor could detect CTCs in the range of 2 to 2×10^6 cells mL^{-1} with a limit of detection 1 cell mL^{-1}. The developed aptasensor, which can simultaneously isolate and detect CTCs, has great application potential in the early monitoring of tumor metastasis and in individualized treatment.

1. Introduction

As a valuable marker of tumor metastasis marker, the detection of circulating tumor cells (CTCs) helps to elucidate the changing trend of the number and type of cancer cells, and provides the basis for dynamic monitoring and treatment evaluation (Goldkorn et al., 2014; Rack et al., 2014). Moreover, the isolation of CTCs contributes to molecular-level research and individualized treatment (Liu et al., 2013; Zhou et al., 2017). Thus, it is of great clinical significance to simultaneously isolate and detect CTCs. Since the number of CTCs in peripheral blood is very low in the early stage of metastasis (Shaffer et al., 2007), the accurate detection and isolation of CTCs has always been a huge challenge.

With the development of CTC research, many advanced analytical methods have been developed and exhibited good performance, including immunology-based methods, microfluidic devices, fluorescent imaging, and cell-adhesion matrix-based platforms (Fass, 2008; Kamyabi et al., 2019; Pearl et al., 2014; Zhang et al., 2002). The CellSearch® system, in particular, has been approved by the U.S. Food and Drug Administration for the treatment of breast cancer and monitoring of prognosis (Huang et al., 2015). Microfluidic chip technology has developed rapidly and has been used for some great breakthroughs in the CTC detection field (Jan et al., 2018). However, these methods are time-consuming, and require expensive instruments, complex operations, and complex manufacturing technology (microarrays and chips), making them unsuitable for a wide range of applications (Ortiz and Yu, 2018; Shields et al., 2015). In recent years, electrochemical biosensors have aroused great interest in the field of laboratory and clinical analysis. For example, Zhou et al. fabricated an electrochemical immunosensor for detection of CTCs using a tyramide signal amplification-based signal enhancement system (Zhou et al., 2019). Cao et al. developed a highly-sensitive electrochemical cytosensor based on DNA-AgNCs (Ag nanoclusters) to detect CTCs (Cao et al., 2019). However, these

* Corresponding author.
E-mail address: liling@cqmu.edu.cn (L. Li).
[1] These authors contributed equally to this work.

https://doi.org/10.1016/j.bios.2020.112516
Received 21 May 2020; Received in revised form 7 August 2020; Accepted 12 August 2020
Available online 28 August 2020

electrochemical sensors can be further improved in terms of isolation of CTCs and sensitivity. There is an urgent need for low-cost, simple, and ultrasensitive methods for the simultaneous isolation and detection of CTCs.

Nanomaterials are widely used in biosensors to improve sensitivity. Previous studies showed that CeO_2 nanomaterials have high catalytic activity similar to horseradish peroxidase (HRP), such as CeO_2 nanoparticles (CeO_2NPs) and CeO_2 nanorods (CeO_2NRs) (Cargnello et al., 2013; Ji et al., 2012; Mai et al., 2015). Besides, Iridium (Ir) has a strong propensity for adsorbing oxygen species. When the Ir is doped, the surface activity of the alloy can increase due to expansion strain (Ford et al., 2010). Li et al. synthesized CeO_2/Ir nanocomposites and verified that the nanocomposites had high catalytic activity (Li et al., 2017). To improve the sensitivity of sensor more efficiently, we designed novel CeO_2@Ir nanorods (Ce@IrNRs) with good dispersion and uniform size. The synthesis and catalytic activity analysis of Ce@IrNRs were a focus of this work.

Enzyme-free DNA walker technology is a new achievement of nucleic acid technology. Compared with traditional DNA walking machine, it does not need track design, labeling, a protease or metalloenzyme, only Mg^{2+}. So, it is simpler, more stable and economical (Cai et al., 2016). With the participation of Mg^{2+}, DNA walker strands (A GCT AGC TAC AAC GA) act as an RNAse to cleave the RNA base of D-RNA (a chimeric DNA/RNA oligonucleotide with a cleavage point rArU). The strands displacement reaction makes the DNA walker strands "walk forward" along the adjacent D-RNA, thereby continuously cleaving D-RNA.

In this work, MCF-7 cells, a breast cancer cell line, were selected as the target cells. They overexpress membrane protein MUC1. MUC1-targeting aptamers with high specificity and affinity were used to recognize MCF-7 cells. Deoxyuracils (dUs) at the end of the aptamer could be specifically hydrolyzed by uracil DNA glycosylase (UDG), which was helpful for isolation of the MCF-7 cells. To amplify the signal, Ce@IrNRs with large surface area and strong peroxidase activity were prepared by *in situ* deposition of Ir on the surface of CeO_2NRs. Ce@IrNRs were then combined with enzyme-free DNA walker technology to achieve dual amplification of the signal, as use of the DNA walker enabled release of a higher number of signal probes. The processes of capturing target cells and releasing signal probes were completed in the liquid phase to improve the efficiency of nucleic acid reaction, and the signal probes, rather than cells themselves, were directly combined with the electrode to reduce the steric hindrance effect (Liu et al., 2018). The results proved that the aptasensor could simultaneously isolate and detection CTCs with high sensitivity and specificity. Therefore, the aptasensor developed in this work can be used for the early monitoring of tumor metastasis and the individualized treatment of cancer.

2. Experiment section

2.1. Materials

All nucleic acid single strands and their modified groups (–biotin, –COOH and $–NH_2$) were synthesized by Sangon Inc. (Shanghai, China). Their sequences are shown in Table S1. DNA marker, streptavidin immunomagnetic beads, $MgCl_2{\cdot}6H_2O$, 1 × TE buffer [10 mM Tris-HCl, 1.0 mM ethylenediaminetetraacetic acid (EDTA), pH 7.5], HRP, 4-dimethylaminopyridine, cerium(III) nitrate hexahydrate, 6-mercapto -1-hexanol (MCH), tris(2-carboxyethyl) phosphine hydrochloride (TCEP), 3, 3′, 5, 5′-tetramethylbenzidine (TMB), polyethylenimine (PEI), 4, 6-diamino-2-phenylindole (DAPI), glutaraldehyde, agarose, UDG, 1-ethyl-3-(3-dimethylaminopropyl) carbodiimide hydrochloride (EDC), and *N*-hydroxysuccinimide (NHS) were purchased from Sangon Inc. All oligonucleotides were dissolved in TE buffer at −20 °C. Tumor cells were suspended in 0.01 M phosphate-buffered saline (PBS, pH 7.4). Water (resistivity, 18.2 MΩ) was purified using a Milli-Q water purification system. Venous whole blood samples were obtained from Chongqing Hospital of Traditional Chinese Medicine.

2.2. Preparation of CeO_2NRs

CeO_2NRs were synthesized according to references (Tian et al., 2015). The synthesis steps were:

Ten milliliters of 173.6 mg mL^{-1} $Ce(NO_3)_3{\cdot}6H_2O$ and 70 mL of 274.3 mg mL^{-1} NaOH were mixed. The mixture of $Ce(NO_3)_3{\cdot}6H_2O$ and NaOH was aged for 30 min at room temperature (RT). After aging, the mixture was treated hydrothermally in a stainless-steel autoclave at ~3.0 atm and 100 °C for 24 h. The product was centrifuged (7104 *g*) for 20 min and washed alternately with ethanol and water three times. The obtained CeO_2NRs were dried at 60 °C overnight and stored at 4 °C until use.

2.3. Preparation of Ce@IrNRs

Thirty-eight milliliters of 1.0 mg mL^{-1} CeO_2NRs suspension was mixed with 4 mL of 1% H_2IrCl_4 solution. After stirring for 30 min, 3 mL of 0.1 M fresh $NaBH_4$ solution was added drop by drop. The reaction was continued for 5 h at 60 °C. The product was centrifuged at 15,984 *g* for 10 min after cooling to RT, and washed alternately with ethanol and water 3–5 times. Finally, the synthetic Ce@IrNRs were stored at 4 °C until use.

2.4. Binding of biotin and carboxyl modified D-RNA to magnetic beads (MBs) and Ce@IrNRs

The binding of D-RNA to MBs was very stable because the MBs were modified with streptavidin and the D-RNA with biotin. Three hundred microliters of 50 μM D-RNA were mixed with 700 μL of 10 mg mL^{-1} MBs. Then, the mixture was stirred at 4 °C for 12 h. After magnetic separation, the MBs/D-RNA were washed three times with deionized water.

Next, MBs/D-RNA/Ce@IrNRs were synthesized according to the method of Ling et al. (2019). First, 1 mg Ce@IrNRs was added to 1% PEI and stirred for 4 h. PEI wrapped Ce@IrNRs were acquired by centrifugation for 15 min at 15,984 *g*. Then, 500 μL of 12.5% glutaraldehyde were added into the Ce@IrNRs/PEI suspension and stirred at RT for 12 h. After centrifugation, Ce@IrNRs/PEI were resuspended for standby. Second, 20 μL of 20 μM MB/D-RNA was mixed with 200 μL NHS (10 mM) and EDC (40 mM) solution for 30 min to activate –COOH groups of the carboxylated D-RNA. Then, 100 μL Ce@IrNRs/PEI was added and stirred at 4 °C for 12 h to produce MB/D-RNA/Ce@IrNR nanocomposites. After centrifugation (7104 *g*, 20 min), the nanocomposites were dispersed in 1 × TE buffer (pH = 7.4) and stored at 4 °C.

2.5. Gel retardation assay

The feasibility of the enzyme-free DNA walker technology was verified by gel retardation assay. Electrophoresis buffer was 1 × TBE (89 mM Tris, 89 mM boric acid, 2 mM EDTA). The agarose concentration was 3%. Electrophoresis was performed at 100 V (constant voltages) for 30 min. The gel was observed under UV light, and a photograph of the gel was analyzed using a gel imaging analysis system (BioRad, USA).

2.6. Preparation of gold electrodes

Gold electrodes with a diameter of 3 mm were polished with 0.3- and 0.05-μm alumina powder at a constant speed to a mirror-like finish. This process lasted about 10 min. The polished gold electrodes were sonicated continuously in ultrapure water, ethanol and ultrapure water for 10 min, respectively. Then, they were activated in the newly prepared piranha solution (98% H_2SO_4: 30% H_2O_2, 3 : 1 v: v) for 5 min. Finally, the gold electrodes were rinsed thoroughly with ultrapure water and dried in air.

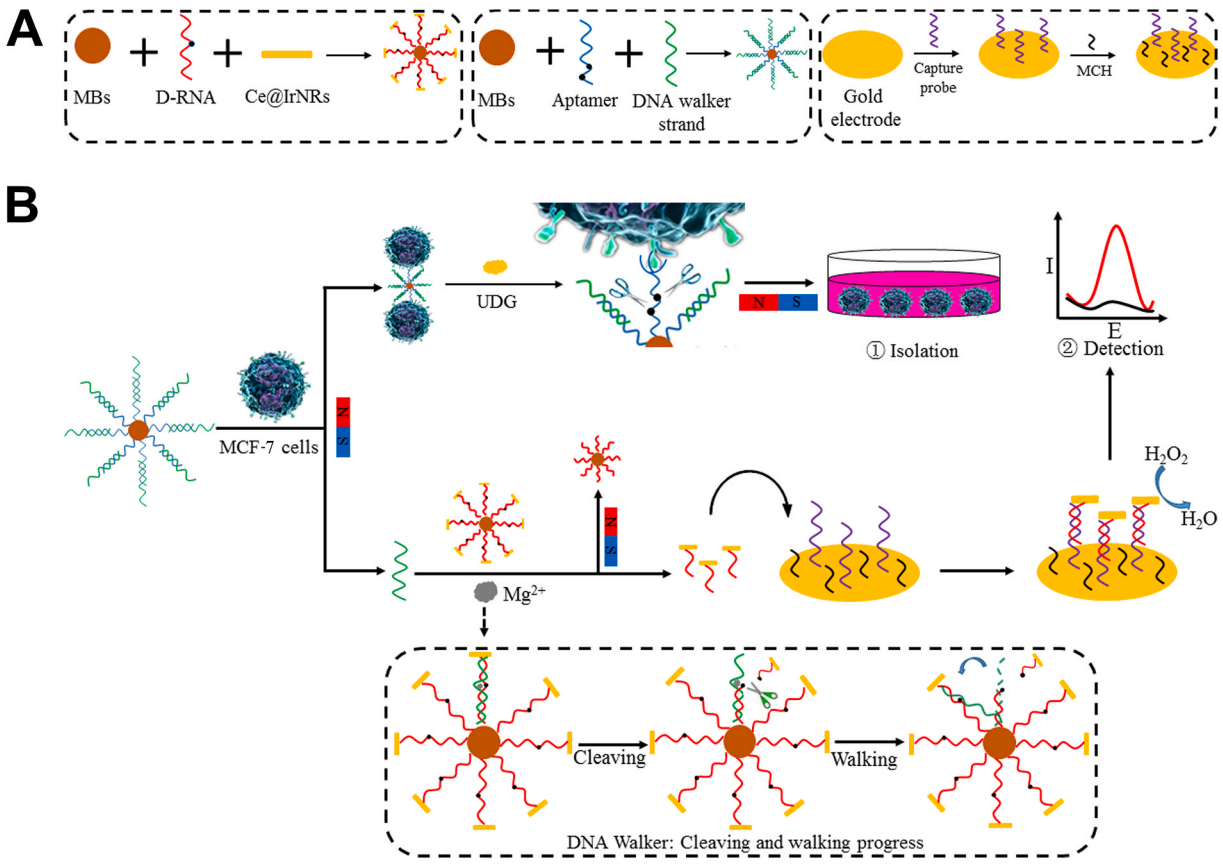

Scheme 1. The principle of electrochemical aptasensor based on Ce@IrNRs and DNA walker for simultaneous isolation and detection of CTCs. (MBs: magnetic beads, UDG: Uracil DNA glycosylase and, MCH：6-mercapto-1-hexanol).

2.7. Self-assembly and characterization of the gold electrode

First, TCEP was used to reduce the disulfide bonds of the thiolated capture probes (the single strands of DNA that capture signal probe) for 120 min at RT in the dark. Subsequently, 10 μL of 2 μM capture probe was dropped on the surface of a polished gold electrode and incubated for 12 h at 4 °C. After rinsing, 10 μL of 10 μM MCH was dropped and incubated for 30 min. Finally, the prepared gold electrodes (MCH/capture probes/gold electrode) were stored at 4 °C.

The self-assembly of the gold electrode was characterized by cyclic voltammetry (CV; from −0.2 to 0.6 V) and electrochemical impedance spectroscopy (EIS; frequency range 10^{-1} – 10^{5} Hz; alternating voltage 5 mV). The working solution contained 5 mM $[Fe(CN)_6]^{3-/4-}$ and 0.1 M KCl.

2.8. Immunofluorescence staining of isolated cells

Briefly, isolated cells were fixed with 4% paraformaldehyde for 30 min (RT), and washed with ice-precooled PBS. Then, they were infiltrated with 0.5% Triton X-100 in PBS for 20 min (RT). After blocking with 0.5% bovine serum albumin (BSA)/PBS for 1 h, they were incubated with fluorescently-labeled antibody [Cy5-labeled anti-MUC1, anti-epidermal growth factor receptor (EGFR) and anti-CD45 antibody] overnight in the dark at 4 °C. Subsequently, they were washed with ice precooled PBS (three times) and dyed with 1 mg mL^{-1} of DAPI in the dark for 10 min at RT. Finally, the stained cells were observed using a fluorescence microscope (Nikon Solar Eclipse 80i).

2.9. Isolation and detection of CTCs

Isolation: 10 μL target cell suspension was added to 200 μL reaction buffer containing 100 nM MBs-aptamer//DNA walker strand. The target cells were specifically captured by the aptamer, while displacing DNA walker strands. Then, the dUs of the aptamer were hydrolyzed by UDG (0.8 U) to release captured target cells. Finally, the isolated target cells were cultured in fresh medium.

Detection: the electrochemical detection was performed in a three-electrode system using CHI660D electrochemical workstation (Chenhua, Shanghai, China). 10 μL of 1 μM MB/D-RNA/Ce@IrNRs was added to the DNA walker strand supernatant from part 1. DNA walker strands continually cleaved D-RNA to release a large number of signal probes. Then, 10 μL of the signal probe supernatant was dropped on the surface of a prepared gold electrode and incubated for 30 min at 37 °C. Finally, differential pulse voltammetry (DPV) was used to measure the current signal in the voltage range of 0.2–0.8 V with a pulse amplitude of 50 mV and a pulse width of 50 ms at 50 mV s^{-1}. The working solution was 100 mM PBS (pH 7.5) containing 1.5 mM H_2O_2 (Scheme 1).

3. Results and discussion

3.1. Characterization of Ce@IrNRs

Transmission electron microscopy (TEM) and scanning electron microscopy (SEM) were used to characterize the morphology of the synthesized nanomaterials. As shown in Fig. 1A, the synthesized nanomaterials were rod-shaped with a diameter of about 13 nm and a length of about 100 nm. High-resolution SEM images (Fig. 1B) clearly showed that there were a large number of fine nanoparticles on the surface of the nanorods. These fine nanoparticles were Ir nanoparticles *in situ* synthesized. The elemental composition of the synthesized materials was analyzed by element mapping. Fig. 1(C - E) showed that the nanomaterials contained a high proportion of Ce and Ir elements, and

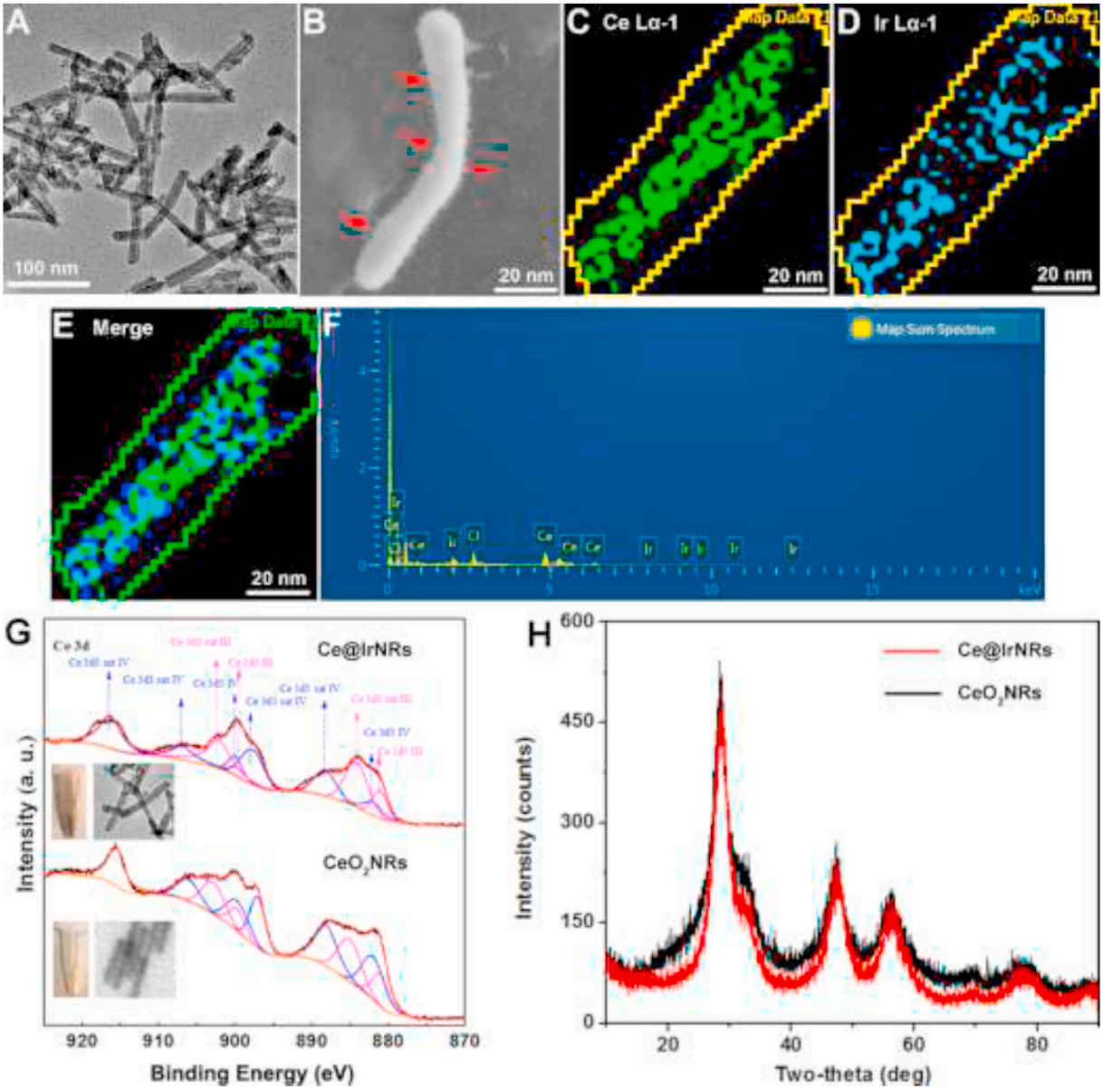

Fig. 1. Characterization of Ce@IrNRs: (A) TEM image of Ce@IrNRs. (B) SEM image of Ce@IrNRs. EDS-mapping images of (C) Ce element, (D) Ir element, and (E) Merge. (F) EDS analysis of Ce@IrNRs. (G) XPS spectra of the Ce 3 d core level regions for Ce@IrNRs and CeO_2NRs. (H) XRD spectra of Ce@IrNRs and CeO2NRs.

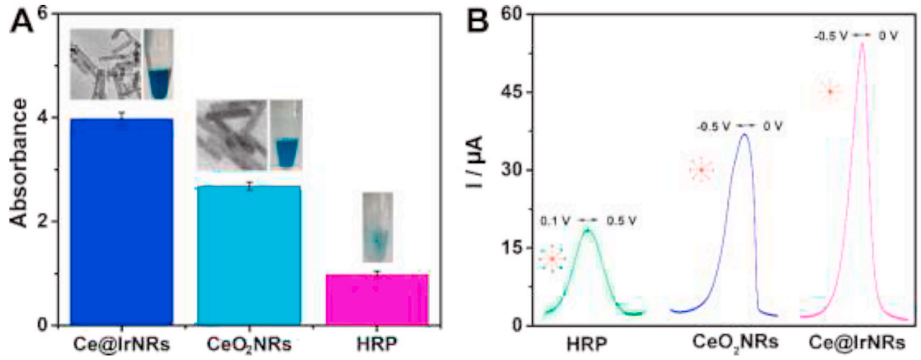

Fig. 2. (A) Comparison of catalytic activity of Ce@IrNRs, CeO_2NRs, and HRP. (B) Comparison of DPV responses of electrochemical aptasensor based on Ce@IrNRs, CeO_2NRs, and HRP.

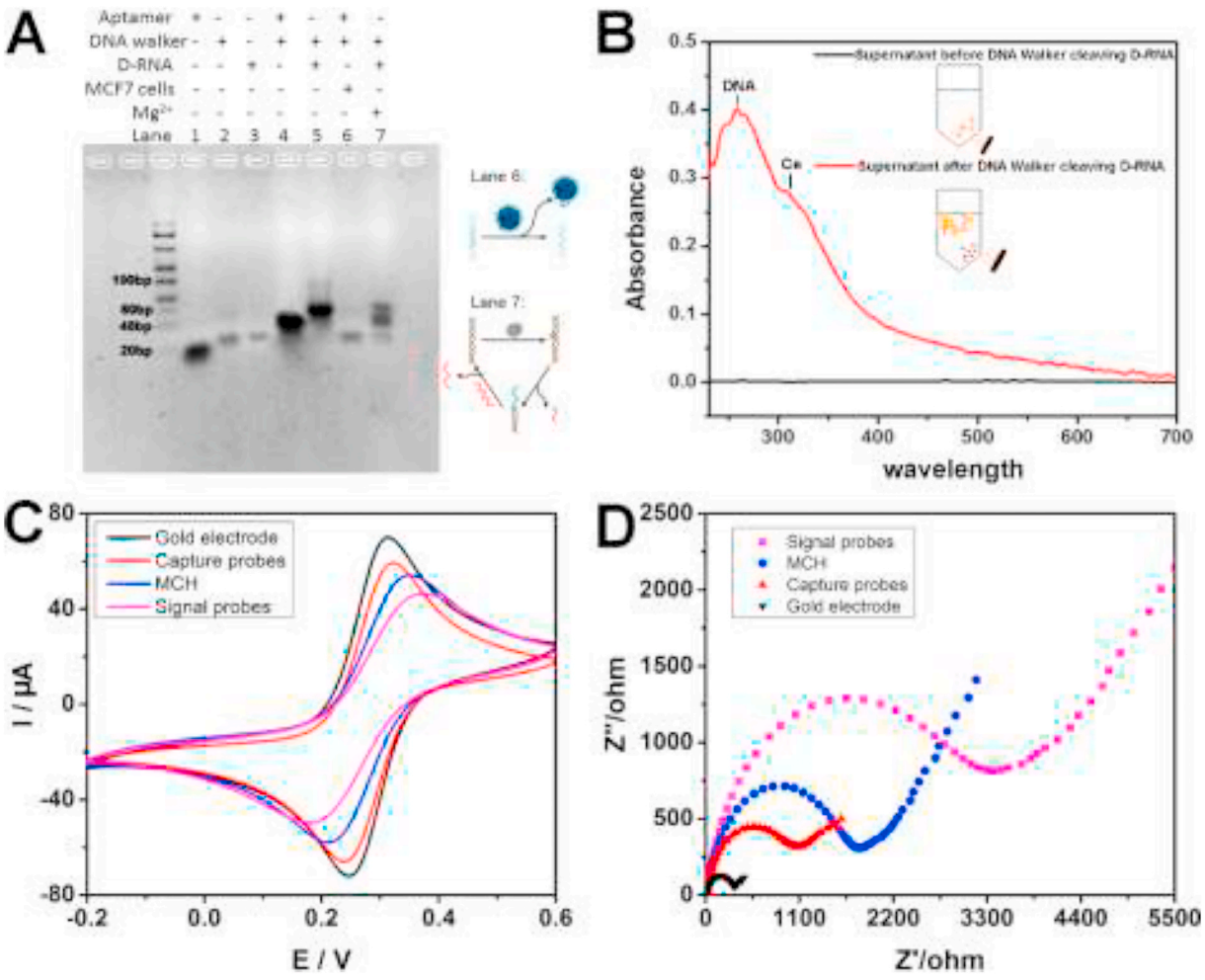

Fig. 3. Verification of the feasibility of enzyme-free DNA walker. (A) Gel retardation assay. (B) UV–Vis analysis of supernatant before and after DNA walker cleaving. Characterization of layer by layer self-assembly on electrode surface. (C) CV and (D) EIS responses: bare gold electrode, capture probes/gold electrode, MCH/capture probes/gold electrode, signal probes/MCH/capture probes/gold electrode. (For interpretation of the references to color in this figure legend, the reader is referred to the Web version of this article.)

these two elements were evenly distributed. In addition, energy dispersive spectrometry (EDS) also clearly showed that the synthesized nanomaterial was mainly composed of Ce and Ir (Fig. 1F). Analysis of the elemental composition and morphological characteristics proved the successful synthesis of Ce@IrNRs.

The chemical state and crystal structure of Ce@IrNRs were analyzed in detail by X-ray photoelectron spectroscopy (XPS) and X-ray diffraction (XRD). Three-dimensional XPS spectra of CeO_2NRs and Ce@IrNRs were shown in Fig. 1G. The peaks in the Ce 3D XPS spectra were divided into two groups. One of these groups was Ce(IV) 3d3 and 3d5, and the other group was Ce(III) 3d3 and 3d5. The XPS original data showed that the surface Ce(III) content of CeO_2NRs was 27.3%, while that of Ce@IrNRs was 39.7%. Previous studies indicated that the content of Ce (III) was related to the defect structure of CeO_2NRs and the formation of oxygen vacancies (Damyanova et al., 2009; Du e al., 2012). Higher content of oxygen vacancies could improve the catalytic activity of CeO_2 nanomaterials (Li et al., 2014). Since oxygen atoms are more likely to bind to Ir, the addition of Ir can promote the conversion of Ce (IV) to Ce (III), thereby increasing the content of oxygen vacancies. Thus, Ce@IrNRs have higher catalytic activity than CeO_2NRs. Moreover, XPS spectra also proved that Ce@IrNRs were successfully synthesized.

As shown in the XRD spectrum (Fig. 1H), the diffraction peak of Ce@IrNRs was more symmetrical, sharper and narrower than that of CeO_2NRs. The results proved that Ce@IrNRs had a larger crystallite size and enhanced crystallinity (Pathak et al., 2019). This was because the *in situ* synthesis of Ir nanoparticles improved the crystal defects of CeO_2NRs and made them larger in size. Therefore, XRD analysis also proved the successful synthesis of Ce@IrNRs.

3.2. Catalytic activity analysis of Ce@IrNRs

The catalytic activity of Ce@IrNRs is closely related to the sensitivity of the aptasensor developed in this study. The catalytic activity of Ce@IrNRs was compared with that of two common catalytic materials (CeO_2NRs and HRP) in the same reaction conditions. As shown in Fig. 2A, in the catalyzed color reaction of TMB, the CeIrNRs group had the darkest color and the highest absorbance. To further prove the advantages, Ce@IrNRs, CeO_2NRs and HRP were respectively used to fabricate the signal probe. Fig. 2B showed that the aptasensor based on Ce@IrNRs had the strongest DPV response. These two results proved that the catalytic activity of Ce@IrNRs was much higher than that of CeO_2NRs and HRP. Therefore, Ce@IrNRs could efficiently improve the sensitivity of the aptasensor.

3.3. Feasibility of the enzyme-free DNA walker technology

The feasibility of the enzyme-free DNA walker technology was verified by gel retardation assay. Fig. 3A showed that DNA walker strands could hybridize with the aptamer and D-RNA respectively to form double strands (lane 4 and 5). Lane 6 showed that MCF-7 cells had

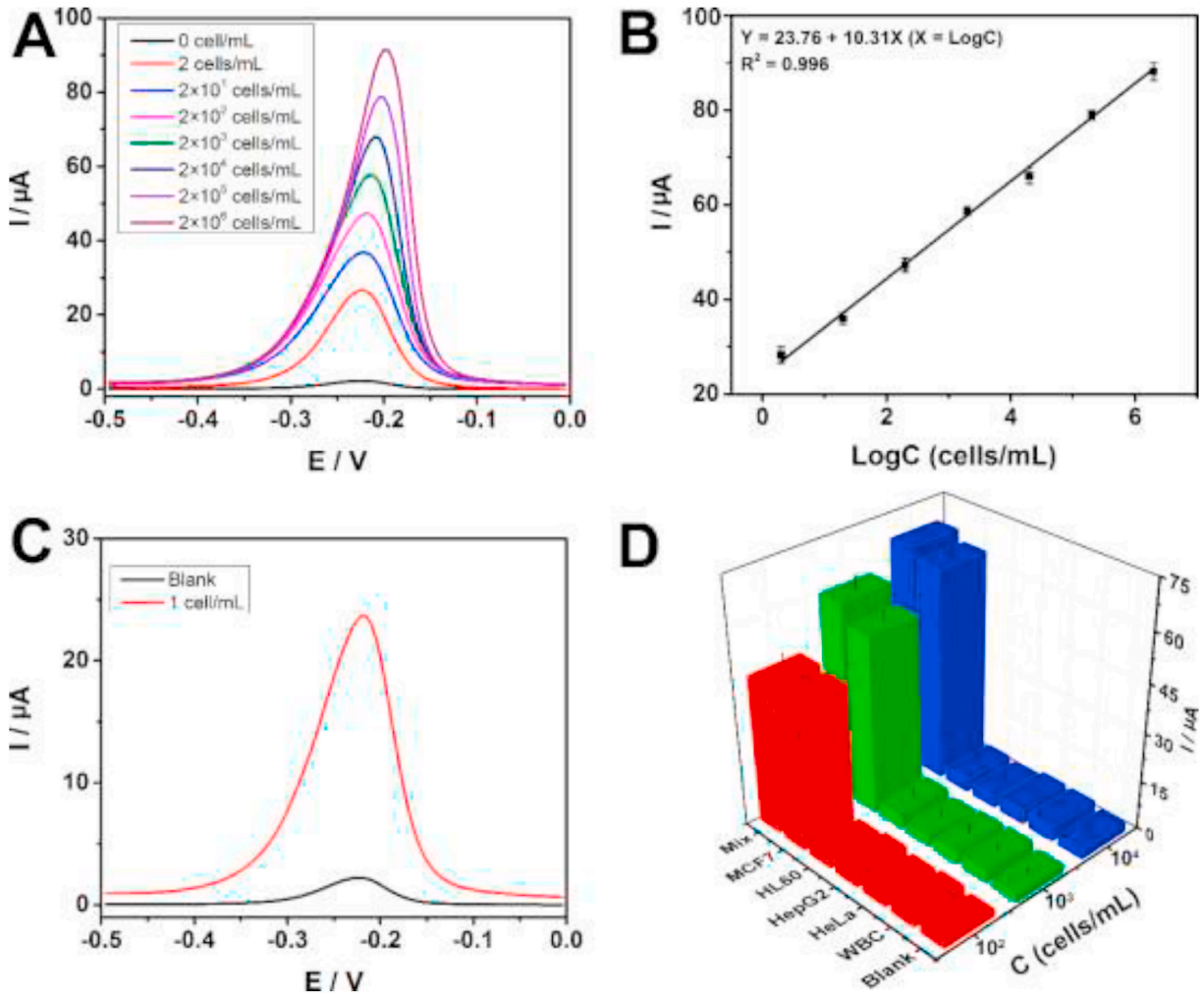

Fig. 4. (A) DPV responses of MCF-7 cells with different concentrations. (B) A linear relationship between the peak currents versus the logarithm of concentrations of MCF-7 cells. (C) DPV response of 1 cells mL^{-1} of MCF-7 cells (LOD). (D) Specificity assessment: Peak current in response to tumor cells (MCF-7, HL60, HeLa and HepG2), normal cells (WBC), and mixture cells (1 : 1: 1 : 1: 1). Error bar = RSD (n = 5).

stronger binding force with the aptamer and could displace the DNA walker strands. Lane 7 showed the results of reaction between the DNA walker strand and the D-RNA in the presence of Mg^{2+}. There are three clear bands in lane 7. The top band represented the double strands formed by the DNA walker strand and the complete D-RNA. The middle band was the double strand formed by DNA walker strands and a cleaved D-RNA fragment. The bottom band was the residual D-RNA fragment after cleavage. Therefore, the enzyme-free DNA walker technology was feasible.

To confirm that the DNA walker strand could effectively cleave D-RNA combined with Ce@IrNRs, UV absorption spectrophotometry and electrochemical methods were used. The D-RNA fragments in the supernatant before and after cleavage and magnetic separation were detected by UV absorption spectrophotometry. As shown in Fig. 3B, there was no absorption peak of DNA in the supernatant before cleavage. However, when Mg^{2+} was added, there were two obvious absorption peaks at 260 nm (DNA) and 330 nm (Ce), which proved that even if D-RNA was combined with Ce@IrNRs and MBs, DNA walker strands could cleave the D-RNA efficiently.

The results of CV and EIS also proved this conclusion (Fig. S1). Because single-stranded nucleic acid can hinder electron transfer, when D-RNA was fixed on the electrode, the current decreased, and the resistance increased. However, when DNA walker strands and Mg^{2+} were added, the current increased and the resistance decreased, which proved that the D-RNA bound to Ce@IrNRs was cleaved efficiently.

3.4. Characterization of self-assembly on the gold electrode

CV and EIS were also used to characterize the layer-by-layer self-assembly on gold electrodes. As shown in Fig. 3C and D, with the capture probes, MCH, and signal probes successively combined on the electrode surface, the current decreased and the resistance increased. This was because the single strand of nucleic acid and the MCH could hinder the transfer of electrons. Therefore, the layer-by-layer self-assembly on the electrodes was successful.

3.5. Optimization of experimental parameters

To obtain the best performance, Mg^{2+} concentration, cleavage and incubation time, temperature, pH, and the capture probe concentration were optimized by DPV response.

Only when Mg^{2+} was present could the DNA walker efficiently cleave D-RNA. Thus, the effect of Mg^{2+} concentration in the range of 5–200 mM was analyzed. As shown in Fig. S2A, when DPV signal was highest, the Mg^{2+} concentration was 100 mM. Next, the effect of DNA walker cleavage time in the range of 5–60 min was assessed. With the prolongation of incubation time, the DPV signal gradually increased and reached a plateau at 30 min (Fig. S2B). The results indicated that 30 min was sufficient to complete the DNA walker cleavage process. In addition, the optimal incubation time for target cells and MBs-Aptamer//DNA walker strand was 35 min and the optimal incubation time for signal

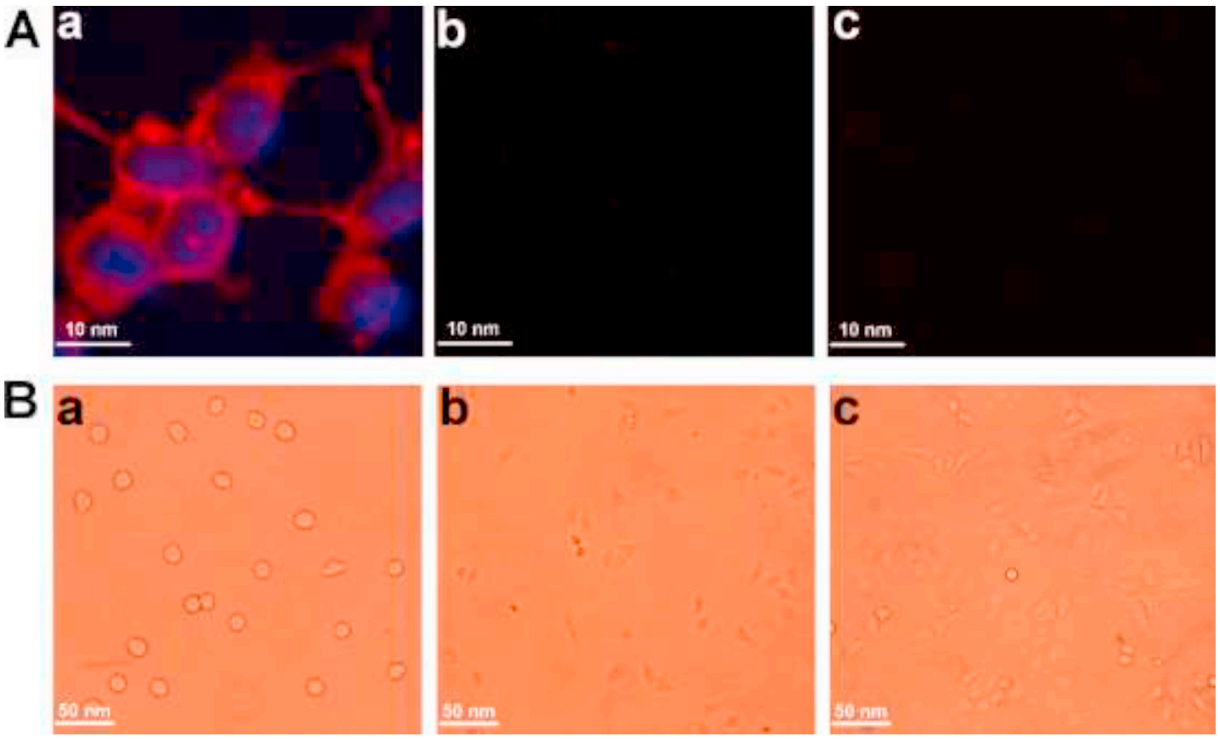

Fig. 5. (A) Isolation specificity assessment. Fluorescence images of the isolated cells: a. MCF-7 cells, b. Hela cells, and c. WBC. (B) Culture of the isolated target cells. Optical microscope images: a. the isolated target cells, b. After culture for 5 h, and c. After culture for 10 h.

probes and electrode was 30 min (Fig. S2C and D). As shown in Fig. S2E, the highest DPV signal proved that the efficiency of DNA walker was the highest at 45 °C. It has been reported that the cleavage event involving DNA walker strands and Mg^{2+} involves catalytic attack on and deprotonation of the 2′-hydroxyl group near the cleavage point of the D-RNA (Cha et al., 2014). The buffer pH has a significant influence on this process. Thus, the pH of the reaction buffer is an essential parameter that needs to be optimized. The effect of pH on the DPV signal was analyzed in the range 5–10. Fig. S2F showed that the signal reached a peak, when pH was 8. The concentration of the capture probe is related to the capture efficiency of signal probes. Low concentrations can result in the inability to capture enough signal probes. However, a high concentration could cause electrostatic repulsion and steric hindrance. The change of DPV response confirmed this hypothesis. As shown in Fig. S2G, between 0.1 and 2 μM, the current signal increases with the increase of the concentration of capture probe and then decreases, and then decreased. The results proved that the optimal concentration of the capture probe was 2 μM.

3.6. Sensitivity and specificity of the electrochemical aptasensor

To evaluate the sensitivity of the aptasensor, a series of concentrations of MCF-7 cells was detected in the optimal experimental conditions established above. The DPV responses with different concentrations of MCF-7 cells were shown in Fig. 4A. The current increased with increasing concentration of MCF-7 cells. The results proved that the aptasensor worked. Moreover, there was a good linear relationship between the current and the logarithm of the number of MCF-7 cells in the range from 2 to 2×10^6 cells mL^{-1} (Fig. 4B). The linear regression equation was: $Y = 23.76 + 10.31X$ ($X = LogC$), $R^2 = 0.996$. According to the limit of detection (LOD) formula: $LOD = 3\sigma/S$ (σ is the linear slope, S is the standard deviation of 11 blank samples), the LOD was estimated to be 1 cell mL^{-1}. As shown in Fig. 4C, the LOD was confirmed (signal to noise ratio > 3). Therefore, the aptasensor had ultra-high sensitivity. Compared with similar methods published in recent years (Cao et al., 2019; Li et al., 2020; Peng et al., 2020), the proposed aptasensor has a great advantage in sensitivity (Table S2).

Moreover, 300 and 3000 cells mL^{-1} were repeatedly detected 11 times, respectively (Fig. S3). The relative standard deviations (RSD) were 1.31% and 1.28%, which indicated the aptasensor had high repeatability. After three aptasensors were stored at 4 °C for 7, 14 and 21 days, 98.3%, 95.8% and 91.7% of the initial DPV responses were retained, respectively (Fig. S4). Therefore, the prepared aptasensor has a long lifetime and good stability.

Next, the specificity of the aptasensor was analyzed. Different kinds of tumor cells were detected using the aptasensor. As shown in Fig. 4D, the current increased sharply only when MCF-7 cells were present. However, for MUC1-negative cells, such as HL-60, HeLa or HepG-2 cells, the current did not change significantly. Therefore, this method not only had high sensitivity and repeatability, but also had high specificity.

3.7. Detection in whole blood samples

To analyze the practical clinical value of the proposed aptasensor, 10, 200 and 1500 MCF-7 cells were added to 1 mL of whole blood from healthy adult females to simulate breast cancer blood samples. DPV responses of these blood samples were shown in Fig. S5. Table S3 showed that the recoveries were 95.6%, 103.4% and 105.5%, respectively. Therefore, the anti-interference properties of the aptasensor could meet the requirements for early screening of CTCs.

To further test its applicability, the developed aptasensor was used to detect MCF7-CTCs in the blood of breast cancer patients at different clinical stages. Fourteen blood samples were collected from six breast cancer patients, two patients in the blast phase of chronic myeloid leukemia (CML), and six healthy adult females (Fig. S6A). As shown in Fig. S6B, the current responses detected using the blood samples from the patients with breast cancer were much higher than those from healthy adult women or those with CML. In addition, the breast cancer blood samples showed different intensities of current signals consistent with the cancer progression stage. These results proved that the

aptasensor could provide a basis for determination of the progression of breast cancer.

3.8. Isolation of the target cells

The isolation of CTCs is very important for the study of individualized medical treatment. The performance of the aptasensor in the isolation of CTCs was evaluated. Firstly, the isolated cells were stained by Cy5-labeled monoclonal antibody to analyze the specificity of the isolation. Fig. 5A showed only MCF-7 cells emitted strong red fluorescence, while nonspecific cells (HeLa and white blood cells) did not emit fluorescence. The results confirmed that the aptasensor had high specificity in the isolation of CTCs.

Subsequently, the isolated cells were cultured in fresh medium. Fig. 5B showed that newly isolated MCF-7 cells dispersed in medium, and had good morphology. After incubation for 5 h, some cells began to adhere to the wall, and proliferated 10 h later. Therefore, the aptasensor could isolate CTCs without them losing biological activity.

4. Conclusions

In summary, an ultrasensitive electrochemical aptasensor was successfully established for simultaneous isolation and detection of CTCs. Novel Ce@IrNRs were synthesized and showed high catalytic activity. Based on the dual signal amplification of Ce@IrNRs and enzyme-free DNA walker technology, the aptasensor could detect CTCs in the range of 2 - 2 $\times$ 10^6 cells mL^{-1}, and the LOD was 1 cell mL^{-1}. Moreover, the aptasensor could accurately identify CTCs in a variety of tumor cell mixtures, and could provide a basis for determining cancer progression by detecting clinical blood samples. More importantly, the aptasensor could isolate the captured CTCs with high specificity without losing cell viability. Therefore, the developed aptasensor not only has great potential for early detection of CTCs, but will also be helpful for individualized research at the molecular and cellular levels. However, it is still a challenge for us to recognize two or more CTC membrane markers simultaneously. Next, the new sensor will combine AND logic and multiple aptamer recognition technology to solve this problem.

CRediT authorship contribution statement

Huawei Shen: Conceptualization, Methodology, Validation, Writing - original draft, Funding acquisition. **Wuquan Deng:** Methodology, Writing - original draft. **Yirui He:** Formal analysis, Writing - original draft. **Xinrun Li:** Investigation, Writing - original draft. **Jinlin Song:** Investigation. **Rui Liu:** Funding acquisition. **Hua liu:** Data curation. **Gangyi Yang:** Resources, Supervision. **Ling Li:** Resources, Supervision, Project administration, Funding acquisition.

Declaration of competing interest

The authors declare that they have no known competing financial interests or personal relationships that could have appeared to influence the work reported in this paper.

Acknowledgments

This work was financially supported by the Natural Science for Youth Foundation, China (No. 81902171 to Huawei Shen, and No. 81300670 to Rui Liu).

Appendix A. Supplementary data

Supplementary data to this article can be found online at https://doi.org/10.1016/j.bios.2020.112516.

References

Cai, S., Chen, M., Liu, M., He, W., Liu, Z., Wu, D., Xia, Y., Yang, H., Chen, J., 2016. Biosens. Bioelectron. 85, 184–189.
Cao, Y., Dai, Y., Chen, H., Tang, Y., Chen, X., Wang, Y., Zhao, J., Zhu, X., 2019. Biosens. Bioelectron. 130, 132–138.
Cargnello, M., Doan-Nguyen, V.V., Gordon, T.R., Diaz, R.E., Stach, E.A., Gorte, R.J., Fornasiero, P., Murray, C.B., 2013. Science 341, 771–773.
Cha, T.G., Pan, J., Chen, H.R., Salgado, J., Li, X., Mao, C.D., Choi, J.H., 2014. Nat. Nanotechnol. 9, 39–43.
Damyanova, S., Pawelec, B., ArishtIrova, K., Huerta, M.V.M., Fierro, J.L.G., 2009. Appl. Catal., B 89, 149–159.
Du, X., Zhang, D., Shi, L., Gao, R., Zhang, J., 2012. J. Phys. Chem. C 116, 10009–10016.
Fass, L., 2008. Mol. Oncol. 2, 115–152.
Ford, D.C., Nilekar, A.U., Xu, Y., Mavrikakis, M., 2010. Surf. Sci. 604, 1565–1575.
Goldkorn, A., Ely, B., Quinn, D.I., Tangen, C.M., Fink, L.M., Xu, T., Twardowski, P., VanVeldhuizen, P.J., Agarwal, N., Carducci, M.A., Monk, J.P., Datar, R.H., Garzotto, M., Mack, P.C., Lara, J.P., Higano, C.S., Hussain, M., Thompson, J.M., Cote, R.J., Vogelzang, N.J., 2014. J. Clin. Oncol. 32, 1136–1142.
Huang, X., Gao, P., Song, Y., Sun, J., Chen, X., Zhao, J., Xu, H., Wang, Z., 2015. BMC Canc. 15, 202.
Jan, Y.J., Chen, J.F., Zhu, Y., Lu, Y.T., Chen, S.H., Chung, H., Smalley, M., Huang, Y.W., Dong, J., Chen, L.C., Yu, H.H., Tomlinson, J.S., Hou, S., Agopian, V.G., Posadas, E. M., Tseng, H.R., 2018. Adv. Drug Deliv. Rev. 125, 78–93.
Ji, Z., Wang, X., Zhang, H., Lin, S., Meng, H., Sun, B., George, S., Xia, T., Nel, A.E., Zink, J.I., 2012. ACS Nano 6, 5366–5380.
Kamyabi, N., Huang, J., Lee, J.J., Bernard, V., Semaan, A., Stephens, B., Hurd, M.W., Vanapalli, S.A., Maitra, A., Guerrero, P.A., 2019. Biomicrofluidics 13, 044111.
Li, J., Zhang, Z.Y., Tian, Z.M., Zhou, X.M., Zheng, Z.P., Ma, Y.Y., Qu, Y., 2014. J. Mater. Chem. 16459–16466.
Li, S., Xu, Y., Chen, Y., Li, W., Lin, L., Li, M., Deng, Y., Wang, X., Ge, B., Yang, C., Yao, S., Xie, J., Li, Y., Liu, X., Ma, D., 2017. Angew. Chem. Int. Ed. 56 (36), 10761–10765.
Li, X., Zhang, P., Dou, L., Wang, Y., Sun, K., Zhang, X., Song, G., Zhao, C., Li, K., Bai, Y., Zeng, X., Zhou, C., Ying, B., Chen, J., Geng, J., 2020. ACS Sens.
Ling, J., Zhao, M., Chen, F., Zhou, X., Li, X., Ding, S., Tang, H., 2019. Biosens. Bioelectron. 127, 167–173.
Liu, G., Ma, C., Jin, B.K., Chen, Z., Zhu, J.J., 2018. Anal. Chem. 90 (7), 4801–4806.
Liu, J., Qin, Y., Li, D., Wang, T., Liu, Y., Wang, J., Wang, E., 2013. Biosens. Bioelectron. 41, 436–441.
Mai, H.X., Sun, L.D., Zhang, Y.W., Si, R., Feng, W., Zhang, H.P., Liu, H.C., Yan, C.H., 2015. J. Phys. Chem. B 51, 24380–24385.
Ortiz, V., Yu, M., 2018. Trends Cell Biol. 28 (10), 764–775.
Pathak, T.K., Kroon, R.E., Craciun, V., Popa, M., Chifiriuc, M.C., Swart, H.C., 2019. Heliyon 5 (3), e01333.
Pearl, M.L., Zhao, Q., Yang, J., Dong, H., Tulley, S., Zhang, Q., Golightly, M., Zucker, S., Chen, W.T., 2014. Gynecol. Oncol. 134, 581–590.
Peng, Y., Tang, S., Shen, H., Sheng, S., Wang, Y., Wang, T., Cai, J., Xie, G., Feng, W., 2020. Mikrochim. Acta 187 (4), 216.
Rack, B., Schindlbeck, C., JÜckstock, J., Andergassen, U., Hepp, P., Zwingers, T., Friedl, T.W., Lorenz, R., Tesch, H., Fasching, P.A., 2014. J. Natl. Cancer Inst. 106.
Shaffer, D.R., Leversha, M.A., Danila, D.C., Lin, O., Espinoza, R.G., Gu, B., Anand, A., Smith, K., Maslak, P., Doyle, G.V., Terstappen, L., Lilja, H., Heller, G., Fleisher, M., Scher, H.I., 2007. Clin. Canc. Res. 13 (7), 2023–2029.
Shields, C.W.T., Reyes, C.D., Lopez, G.P., 2015. Lab Chip 15 (5), 1230–1249.
Tian, Z., Li, J., Zhang, Z., Gao, W., Zhou, X., Qu, Y., 2015. Biomaterials 59, 116–124.
Zhang, J., Campbell, R.E., Ting, A.Y., Tsien, R.Y., 2002. Nat. Rev. Mol. Cell Biol. 3, 906–918.
Zhou, L.L., Dicker, D.T., Matthew, E., El-DeIry, W.S., Alpaugh, R.K., 2017. F1000research 6, 1445.
Zhou, X.Y., Li, Y.J., Wu, H.P., Huang, W., Ju, H.X., Ding, S.J., 2019. Biosens. Bioelectron. 130, 88–94.